Particle Acceleration in Solar Flares and Enrichment of ^{3}He and Heavy Ions

Vahé Petrosian[1,2,3]

ABSTRACT

We discuss possible mechanisms of acceleration of particles in solar flares and show that turbulence plays an important role in all the mechanism. It is also argued that stochastic particle acceleration by turbulent plasma waves is the most likely mechanism for production of the high energy electrons and ions responsible for observed radiative signatures of solar flares and for solar energetic particle or SEPs, and that the predictions of this model agrees well with many past and recent high spectral and temporal observations of solar flares. It is shown that, in addition, the model explains many features of SEPs that accompany flares. In particular we show that it can successfully explain the observed extreme enhancement, relative to photospheric values, of ^{3}He ions and the relative spectra of ^{3}He and ^{4}He. It has also the potential of explaining the relative abundances of most ions including the increasing enhancements of heavy ions with ion mass or mass-to-charge ratio.

1. Introduction

The aim of this paper is to investigate to what extent current theoretical models of acceleration of particles can explain the observed characteristics of solar energetic particles (SEPs), in particular the extreme enhancement, relative to photospheric values, of ^{3}He ions in many flares, in particular in the so-called impulsive (or He-rich) events. In the next section we present a general description of the possible acceleration mechanisms for production of particles in solar flare. We show that plasma waves or turbulence play a major role in all these processes. In §3 we describe the model of stochastic acceleration by plasma turbulence in some detail and review its successes in describing observations of solar flares, in particular the radiative signatures produced by accelerated electrons and protons. In §4 we address the problem of observed enhancements of ^{3}He and heavy elements. Here we first present a brief review of some of the earlier models proposed for production of these enhancements and then compare predictions of the stochastic acceleration model with the observations. A brief summary and discussion is presented in §5.

[1]Department of Physics, Stanford University, Stanford, CA, 94305 email; vahep@stanford.edu

[2]Kavli Institute for Particle Astrophysics and Cosmology, Stanford University, Stanford, CA 94305

[3]Also Department of Applied Physics

2. Particle Acceleration

In this section we first compare various acceleration processes and stress the importance of plasma wave turbulence (**PWT**) as an agent of acceleration, and then describe the basic scenario and equations for treatment of these processes in the stochastic acceleration (**SA**) model. As described below there is growing evidence that PWT plays an important role in acceleration of particles in general, and in solar flares in particular. The two most commonly used acceleration mechanisms are the following.

1. Electric Field Acceleration: Electric fields parallel to magnetic fields can accelerate charged particles. For solar flare conditions the Dreicer field $\mathbf{E}_D = k_B T/(ev\tau_{\rm Coul}) \sim 10^{-5}$ V/cm. (Here k_B, T, v and e are the Boltzmann constant, plasma temperature, particle velocity and charge, and $\tau_{\rm Coul}$ is the mean collision time.) Sub-Dreicer fields ($\mathbf{E} \leq \mathbf{E}_D$) can only accelerate particles up to 10's of keV (for a typical flare length scale $L \sim 10^9$ cm) which is far below the 10's of MeV electrons or > 10 GeV protons required by observations[1]. Super-Dreicer fields, which seem to be present in many simulations of reconnection (Drake, 2006, see also Cassak et al. 2006; Hoshino 2006, see also Zenitani & Hoshino, 2005), accelerate particles at a rate that is faster than $\tau_{\rm Coul}$. This can lead to a runaway and an unstable electron distribution which, as shown theoretically, by laboratory experiments and by the above mentioned simulations, most probably will give rise to PWT (Boris et al. 1970, Holman 1985)[2]. *In summary the electric fields arising as a result of reconnection cannot be the sole agent of acceleration, but may produce an unstable particle momentum distribution which will produce PWT that can then accelerate particles.*

2. Fermi Acceleration: Nowadays this process has been divided into two kinds. In the original Fermi process particles of velocity v scattering randomly with a (pitch angle cosine μ) diffusion rate $D_{\mu\mu}$ by moving scattering agents with a velocity u gain energy at a rate proportional to $(u/v)^2 D_{\mu\mu}$. This, known as a *second order Fermi process*, is what we call *stochastic acceleration* (**SA**). *For solar flares the most likely agent for scattering is PWT.* An alternative process is what is commonly referred to as **Shock** acceleration. Because particles crossing the shock (or any kind of flow convergence) gain energy at a rate which is $\propto u_{sh}/v$, this is known as the *first order Fermi* process. Ever since the demonstration by several authors that a very simple version of this process leads to a power law spectrum that agrees approximately with observations of the cosmic rays, shock acceleration is commonly invoked in space and astrophysical plasmas. However, this simple model, though very elegant, has many shortcomings Specially when applied to non-thermal radiation processes.

Shock acceleration, as commonly used, requires injection of (sometimes high energy) particles and is unable to accelerate low energy background particles. The simple results also break down

[1]Dreicer field will be large if the resistivity and density are anomalously high (Tsuneta 1985; Holman 1996a, b).

[2]Note also that production of a broad power-law requires a wide range of potential drops (Litvinenko, 2003).

when one considers more realistic models. For example, inclusion of losses (Coulomb at low energies and synchrotron at high) or influence of accelerated particles on the shock structure (see *e.g.* Ellison et al. , 2005: Amato & Blasi 2005) cause breaks and generally deviations from a simple power law. More importantly, a *shock by itself cannot accelerate particles* and requires some scattering agents (most likely PWT) to cause repeated passages of the particles through the shock front (thus the name Fermi). The rate of energy gain is governed by the scattering rate $D_{\mu\mu}$. This is the case for the so-called quasi-parallel shock, but shocks are most likely quasi-perpendicular in which case, as pointed out by Jokipii (*e.g.* 1987), the particles may drift along the surface of the shock and get accelerated more efficiently. However, this model also suffers from the above mentioned fundamental limitation and requires injection of particles with velocities $v > u_{sh}\eta$, where $\eta \gg 1$ is the ratio of parallel to perpendicular (to magnetic field) diffusion coefficients. In a more recent simulation of this process Giacolone (2005) shows that a non-thermal tail can be produced from a thermal distribution. However, this model includes significant field fluctuations, which as advocated below can accelerate low energy particles more efficiently than shocks. Thus, it is not obvious what are the relative roles of shock vs SA here. Moreover, for solar flares there is no direct evidence for shocks near the LT during the impulsive phase, and some of the features that make acceleration of cosmic rays by shocks attractive are not present[3].

Stochastic Acceleration is favored because the PWT needed for scattering can also accelerate particles stochastically with the rate D_{EE}/E^2, so that shocks may not be always necessary. First, contrary to common belief, Hamilton & Petrosian 1992 and Miller & Reames 1996 have shown that for flare conditions PWT can accelerate the background particles to high energies within the desired time. More importantly, at low energies or in strongly magnetized plasmas the acceleration rate D_{EE}/E^2 may exceed the scattering rate $D_{\mu\mu}$ (see Pryadko & Petrosian, **PP97**). *Thus, for flare conditions low energy particles are accelerated more efficiently by PWT than by shocks.* We note, however, that in gradual flares there may be a need for a second stage acceleration of SEPs by high coronal shocks[4].

Irrespective of which process dominates the particle acceleration, it is clear that PWT has a role in all of them. Thus, understanding of the production of PWT and its interaction with particles is extremely important. Moreover, **turbulence** is expected to be present in most astrophysical plasmas including solar flares and in and around interplanetary shocks, because the ordinary and magnetic Reynolds numbers for these situations are very large and may be the most efficient channel of energy dissipations in non-equilibrium systems such as solar flares. In recent years there has been a substantial progress in the understanding of MHD turbulence (Goldreich & Sridhar, 1995, 1997;

[3]For example, acceleration by sub Alfvénic shocks is questionable (see Kulsrud 2005), and the streaming instability, which is a part of the traditional shock acceleration can be partially suppressed in the presence of PWT (Yan & Lazarian 2002; Farmer & Goldreich 2004).

[4]In practice, *i.e.* mathematically, there is little difference between the two mechanisms (Jones 1994), and the acceleration by turbulence and shocks can be combined (see below).

Lithwick & Goldreich 2001; Cho & Lazarian 2002 and 2006). These advances provide new tools for a more quantitative investigation of turbulence and the role it plays in solar flares.

3. Stochastic Acceleration and Solar Flares

3.1. Basic Scenario

The complete picture of a solar flare involves many phases or steps. After a complex pre-flare buildup, the first phase is the reconnection or the energy release process. The final consequences of this released energy are the observed radiations (from long wavelength radio to GeV gamma-rays), SEPs and CMEs. Many processes are involved in conversion of the released energy into radiation. As stressed above we believe that PWT plays an important role in these processes. We envision the following scenario. Magnetic energy is converted into turbulence by the reconnection process above corona loops which we refer to as the acceleration site or the loop top (**LT**) source (see Figure 4). The turbulence or waves generated on some macroscopic scale (some fraction of reconnection site scale) undergo two kind of interactions. The first is *nonlinear wave-wave interaction* causing them to undergo dissipationless cascade to smaller scales. The second is *wave-particle interaction* which becomes more important at smaller scales. This damps the turbulence. The lost energy goes into heating the background plasma and/or accelerating particles into a non-thermal tail. The accelerated particles on the open field lines escape the Sun and are observed as SEPs having undergone varied degree of scatterings and acceleration (*e.g.* by interplanetary shocks) during their transport to the Earth. The escaping electrons may also produce type III radio bursts. The particles on the field lines associated with the closed loops spiral down towards the photosphere and produce the observed non-thermal radiations via their interactions with the background particles (and fields) along the loop and primarily at the footpoints (**FPs**). However, most of the energy of the non-thermal particles is lost by collisions causing heating and evaporation of the colder chromospheric plasma, which is responsible for most of the softer thermal radiation. This process, described by the hydrodynamic equations, has a time-scale comparable to the sound travel time, and is somewhat decoupled from the acceleration-transport process that has a much shorter time-scale. However, the evaporation can modulate the high energy processes by changing the density and temperature in the acceleration site.

3.2. Formalism

The mathematical treatment of the processes involved in such a scenario is long and complex. Below we give an outline of the important aspects.

3.2.1. Kinetic Equations

The spectrum of PWT $W(\mathbf{k},t)$ is determined by the wave-wave and wave-particle interactions. The cascade is evaluated from the rates of wave-wave interactions. For example the three wave interactions can be presented as (see *e.g.* Chandran 2005; Luo & Melrose 2006)

$$\omega(\mathbf{k}_1)+\omega(\mathbf{k}_2)=\omega(\mathbf{k}_3) \quad \text{and} \quad \mathbf{k}_1+\mathbf{k}_2=\mathbf{k}_3, \tag{1}$$

where ω and $\mathbf{k}$ are the wave frequency and wavevector. The interaction rates can be represented by the wave diffusion coefficient D_{ij}. In general, at large scales the cascade time $\tau_{\rm cas}\sim k^2/D_{ij}$ is shorter than the damping time $\Gamma(k)^{-1}$ resulting from wave-particle interactions. Thus, the waves undergo dissipationless cascade from the injection scale $k_{\rm min}\sim L^{-1}$ (with a rate $\dot{Q}^W(\mathbf{k})$) till $k_{\rm max}$ where $\tau_{\rm cas}\Gamma=1$, known as the *inertial range*. Beyond $k_{\rm max}$ the spectrum of waves drops off more rapidly. Adopting the diffusion approximation (see *e.g.* Zhou & Matthaeus 1990), one can obtain the evolution of the spatially integrated wave spectrum $W(\mathbf{k},t)$

$$\frac{\partial W}{\partial t}=\frac{\partial}{\partial k_i}\left[D_{ij}\frac{\partial}{\partial k_j}W\right]-\Gamma(\mathbf{k})W-\frac{W}{T^W_{\rm esc}(\mathbf{k})}+\dot{Q}^W. \tag{2}$$

We will assume that all the wave energy is absorbed so that there is no wave escape, *i.e.* $T^W_{\rm esc}\rightarrow\infty$.

The general equation for treatment of the **particle acceleration and transport** is the Fokker-Planck equation for the gyro-phase averaged particle distribution $f(t,s,E,\mu)$ as a function of distance s along the magnetic field lines. This equation is simplified considerably if one can adopt the isotropic approximation (or deal with the pitch-angle averaged distribution) and impose the homogeneity condition (or deal with distribution integrated over the acceleration region). These are reasonable assumptions for particles at the flare site and amount to determination of the evolution of the energy spectrum $N(E,t)=\int\int d\mu ds f(t,s,E,\mu)$:

$$\frac{\partial N}{\partial t}=\frac{\partial}{\partial E}\left[D_{EE}\frac{\partial N}{\partial E}-(A-\dot{E}_L)N\right]-\frac{N}{T^p_{\rm esc}}+\dot{Q}^p, \tag{3}$$

Here $D_{EE}/E^2, A(E)/E$ describe the energy diffusion and direct acceleration rates. They are obtained from consideration of the wave-particle interactions, which are often dominated by resonant interactions, specially for low beta (magnetically dominated) plasma, such that

$$\omega(\mathbf{k})-k\cos\theta v\mu=n\Omega/\gamma, \tag{4}$$

for waves propagating at an angle θ with respect to the large scale magnetic field, and a particle of velocity v, Lorentz factor γ, pitch angle cosine μ and gyrofrequency Ω. Here the harmonic number n (not to be confused with the density) is equal to zero for transit time damping (**TTD**) process. For parallel propagating waves (**PPWs**) $n=\pm1$ but for obliquely propagating waves $n=\pm1,\pm2,....$ $\dot{E}_L/E$ is the energy loss rate of the particles (due mainly to Coulomb collisions and synchrotron losses) and $\dot{Q}^p$ and the terms with the escape times $T_{\rm esc}$ describe the source and leakage of particles.

(For a more detailed discussion leading to the above equations see Miller et al. 1996 and Petrosian & Liu 2004, **PL04**).

The above two kinetic equations are coupled by the fact that the coefficients of one depend on the spectral distribution of the other. Conservation of energy requires that the energy lost by the waves $\dot{\mathcal{W}}_{\rm tot} \equiv \int \Gamma(\mathbf{k}) W(\mathbf{k}) d^3k$ be equal to the energy gained by the particles from the waves; $\dot{\mathcal{E}} = \int [A(E) - A_{\rm sh}] N(E) dE$. Representing the energy transfer rate between the waves and particles by $\Sigma(\mathbf{k}, E)$ this equality implies that

$$\Gamma(\mathbf{k}) = \int_0^\infty \dot{E} N(E) \Sigma(\mathbf{k}, E), \quad A(E) = \int_0^\infty d^3k W(\mathbf{k}) \Sigma(\mathbf{k}, E) + A_{\rm sh} \ , \tag{5}$$

where we have added $A_{\rm sh}$ to represent contributions of other (non-SA) processes affecting the direct acceleration, *e.g.* shocks.

The transport effects and further acceleration of the particles as they travel in the interplanetary space can also be treated by similar equations.

3.2.2. Dispersion Relations

At the core of the evaluation of all the coefficients of the kinetic equations described above lies the plasma dispersion relation $\omega(\mathbf{k})$ which determines the characteristics of the waves that can be excited in the plasma, and the rates of wave-wave and wave-particle interactions. For example, in the MHD regime for a cold plasma

$$\omega = v_{\rm A} k \cos\theta \quad \text{and} \quad \omega = v_{\rm A} k \tag{6}$$

for the Alfvén and fast magneto-sonic waves, respectively, where $v_{\rm A}$ is the Alfvén velocity. Beyond the MHD regime a multiplicity of wave modes can be present and the dispersion relation is more complex and is obtained from the following expressions:

$$\tan^2\theta = \frac{-P(n_r^2 - R)(n_r^2 - L)}{(Sn_r^2 - REL)(n_r^2 - P)} \tag{7}$$

where $n_r = kc/\omega$ is the refractive index, $S = \frac{1}{2}(R + L)$, and

$$P = 1 - \sum_i \frac{\omega_{pi}^2}{\omega^2}, \quad R = 1 - \sum_i \frac{\omega_{pi}^2}{\omega^2} \left(\frac{\omega}{\omega + \epsilon_i \Omega_i} \right), \quad \text{and} \quad L = 1 - \sum_i \frac{\omega_{pi}^2}{\omega^2} \left(\frac{\omega}{\omega - \epsilon_i \Omega_i} \right). \tag{8}$$

Here $\omega_{pi}^2 = \frac{4\pi n_i q_i^2}{m_i}$ and $\Omega_i = \frac{|q_i| B}{m_i c}$ are the plasma and gyro frequencies, $\epsilon_i = \frac{q_i}{|q_i|}$, and n_i, q_i, and m_i are the density, charge, and mass of the background particles (electron, proton and α.) Figure 1 shows the more complete picture of the dispersion surfaces (depicted by the curves) obtained from the well known cold plasma expressions along with the resonant planes in the (ω, $k_\parallel$, $k_\perp$)

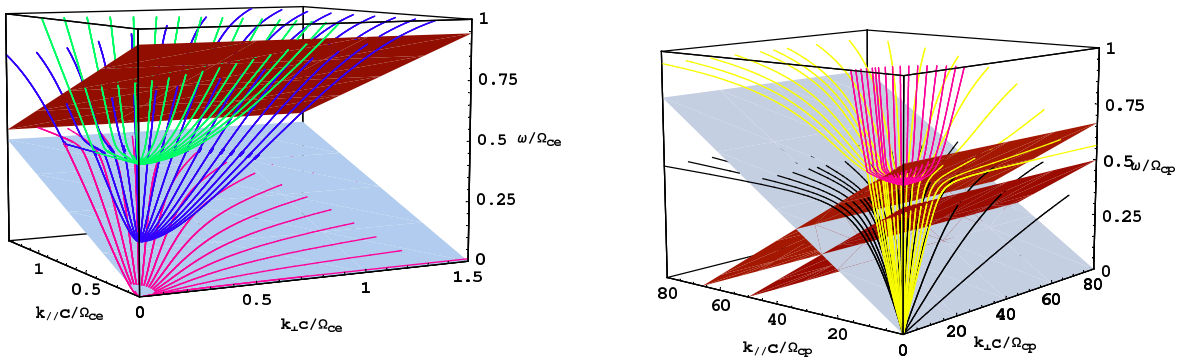

Fig. 1.— Dispersion relation (curves) and resonance condition (flat) surfaces for a cold fully ionized H and He (10% by number) plasma with $\beta_{\rm A} = v_{\rm A}/c = 0.012$ showing the regions around the electron (left) and proton (right) gyro-frequencies. Only waves with positive $k_\parallel, k_\perp$ (or $0 < \theta < \pi/2$) are shown. The mirror image with respect to the (ω, $k_\perp$) plane gives the waves propagating in the opposite direction. From high to low frequencies, we have one of the electromagnetic branches (green), upper-hybrid branch (purple), lower-hybrid branch, which also includes the whistler waves (pink), fast-wave branches (yellow), and Alfvén branch (black). The effects of a finite temperature modify these curves at frequencies $\omega \sim k v_{\rm th}$, where $v_{\rm th} = \sqrt{2k_{\rm B}T/m}$ is the thermal velocity (see *e.g.* André 1985). The resonance surfaces are for electrons with $v = 0.3c$ and $|\mu| = 1.0$ (left: upper $n = 1$, lower $n = 0$) and ^{4}He (right: middle $n = 1$) and ^{3}He (right: upper $n = 1$) ions with $|\mu| = 1.0$ and $v = 0.01c$. The resonance surfaces for the latter two are the same when $n = 0$ (right: lower).

space. Intersections between the dispersion surfaces and the resonant planes define the resonant wave-particle interactions.

The above dispersion relations are good approximations for low beta plasmas,

$$\beta_p = 2(v_s/v_{\rm A})^2 = 8\pi n k_{\rm B} T/B^2 = 3.4\times10^{-2}(n/10^{10}{\rm cm}^{-3})(100{\rm G}/B)^2(T/10^7{\rm K}) \ll 1, \qquad (9)$$

where $v_s = \sqrt{k_{\rm B}T/m_p}$ is the sound speed. For higher beta plasmas, *e.g.* at higher temperatures, these relations are modified, specially for higher frequencies $\omega \sim k v_{\rm th}$, where $v_{\rm th} = \sqrt{2k_{\rm B}T/m}$. For example, in the MHD regime, in addition to the Alfvén mode one gets fast and slow modes with the dispersion relation (see *e.g.* Sturrock 1994)

$$(\omega/k)^2 = \frac{1}{2}\left[(v_{\rm A}^2 + v_s^2) \pm \sqrt{v_{\rm A}^4 + v_s^4 - 2v_{\rm A}^2 v_s^2 \cos 2\theta}\right], \qquad (10)$$

and the more general dispersion relation is modified in a more complicated way (see *e.g.* André 1985 or Swanson 1989). The finite temperature imparts an imaginary part to the wave frequency that gives the (Landau) damping rate of the waves (see *e.g.* Swanson 1989 or Pryadko & Petrosian 1998, 1999 and Cranmer & van Ballegooijen 2003 for application to solar flare conditions). In general, these rates and the modification of the dispersion relation are known for Maxwellian (sometimes anisotropic) energy distribution of the plasma particles. For non-thermal distributions the damping rates can be evaluated as described in Petrosian, Yan & Lazarian (2006) using the coupling described in equation 5. If the damping due to non-thermal particles is important then the wave and particle kinetic equations (2) and (3) are coupled. This will be important in large intense flares where a

substantial fraction of particles are accelerated into a non-thermal tail. However, most often the damping rate is dominated by the background thermal particles so that the wave and non-thermal particle kinetic equations decouple. This simplifies matters considerably. One can then use the imaginary part of the wave frequency for evaluation of the damping rate using the well-known hot plasma dispersion relation. Moreover, the 'thermal' effects change the real part of the wave frequency only slightly so that often the real part (and the particle diffusion coefficients) can be evaluated using the simpler cold plasma dispersion relation depicted in Figure 1.

3.2.3. Some Model Results

We now demonstrate some of the basic characteristics of our scenario which can be compared with observations. The complete treatment of the problem requires solution of the coupled wave particle kinetic equations for particles at all energies and pitch angles and waves propagating at all angles. In principle, given the plasma density, magnetic field, temperature (n, B, T), the geometry of the region (represented by a size L here), the rate and scale of injection of turbulence $\dot{Q}^W(\mathbf{k},t)$, one can evaluate the coefficients of equations (2) and (3) and solve the coupled kinetic equations for determination of the resultant distributions $N(E,t)$ and $W(\mathbf{k},t)$. However, under certain circumstances some simplifications are possible. As mentioned above in most cases the damping by non-thermal particles can be ignored and the equations are decoupled. The wave spectrum then can be approximated by a power law in the inertial range ($W \propto k^{-q}, k_{\rm min} < k < k_{\rm max}$) with a steeper falling spectrum beyond this range. The exponent q will be in the range expected in a Kolmogorov or Kraichnan cascade. Furthermore, as shown in Petrosian et al. (2006), the upper limit $k_{\rm max}$ depends strongly on the angle of propagation θ with only quasi-parallel propagating waves **PPWs** reaching small enough scale to be in resonant with low energy particles. Thus, the initial acceleration of thermal particles will be dominated by such waves. Consequently, in what follows here and the next section we assume PPWs with the above spectrum. The following results are based on PL04, where more details can be found.

The left panel of Figure 2 shows the dispersion relation for PPW and the resonant conditions (straight lines) for an electron and a proton of the specified energy and pitch angle cosine. The main parameter determining these curves and the resulting resonances (intersections of the lines with the curves) is the ratio of the plasma to gyro frequencies

$$\alpha = \omega_{pe}/\Omega_e = (m_e/m_p)^{1/2}/\beta_{\rm A} = 3.2(n/10^{10}{\rm cm}^{-3})^{1/2}(100{\rm G}/B). \quad (11)$$

The right panel of Figure 2 shows the timescales associated with the terms in equation (3), *i.e.* loss time $\tau_{\rm loss} = E/\dot{E}_L$, diffusion time $\tau_{\rm diff} \sim E^2/D_{EE}$, acceleration time $\tau_{\rm a} = E/A(E)$, and escape time[5] $T_{\rm esc} = T_{\rm cross}(1 + T_{\rm cross}/\tau_{\rm scat})$.

[5]This is an approximate relation valid for scattering time $\tau_{\rm scat} \lesssim D_{\mu\mu}^{-1}$ > longer and shorter than $T_{\rm cross} \sim L/v$, the

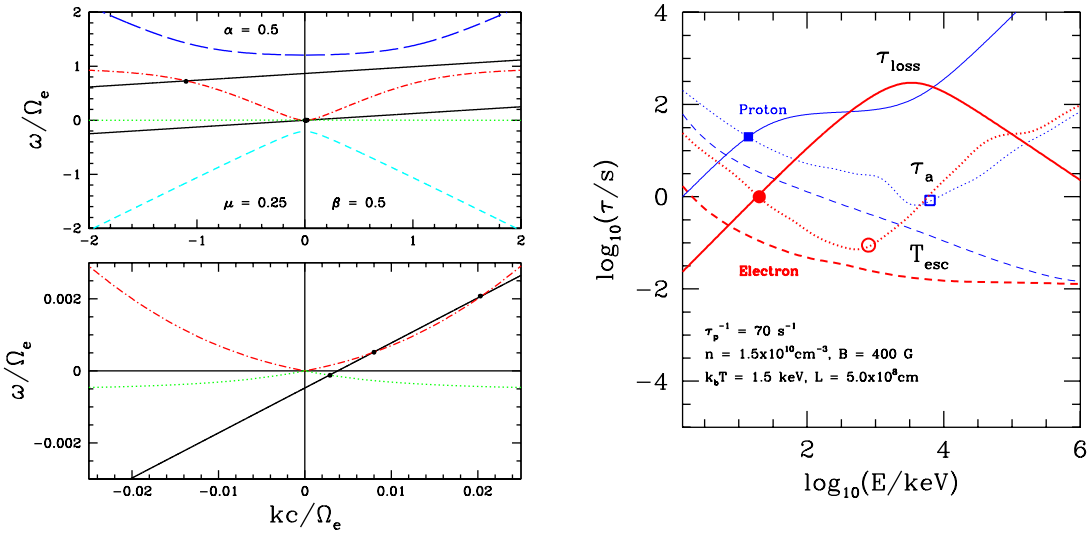

Fig. 2.— **Left panel:** The dispersion relation for PPWs (curves) and the resonant relation (lines, from eq.[4]) for electrons (top) and protons (bottom, expanded near the origin). Note that the resonant lines start (at $k = 0$) from the gyro frequency of the particle (divided by the Lorentz factor $\gamma \sim 1$). **Right panel:** Time scales for a SA acceleration model for solar flare conditions and an assumed spectrum of PWT. Model parameters are indicated in the figure ($\tau_p^{-1} \propto \Omega_e \mathcal{W}/B^2$ is a characteristic wave-particle interaction rate and $\alpha \propto \sqrt{n}/B$). The acceleration, escape, and loss times are indicated by the dotted, dashed, and solid curves, respectively. The thick (red) curves are for electrons and thin (blue) curves are for protons.

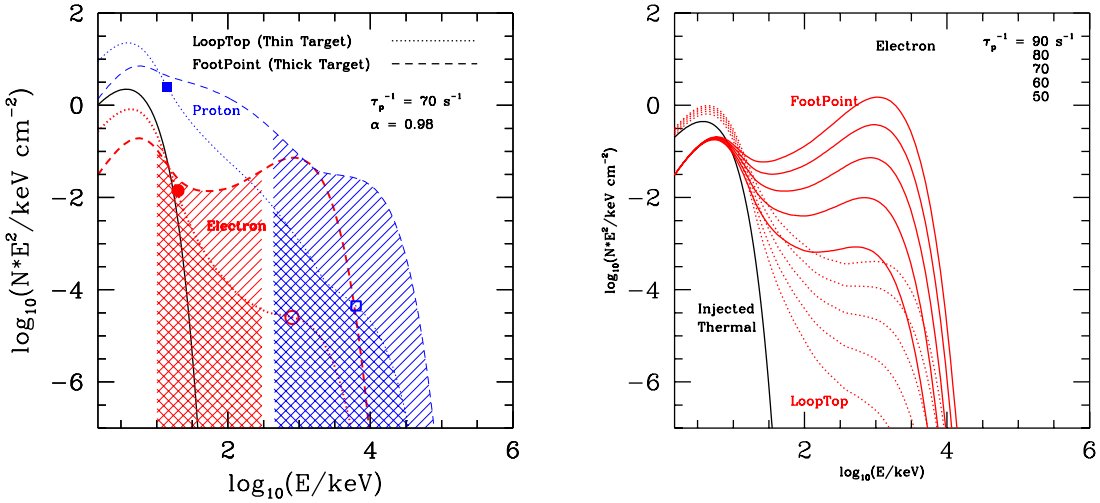

Fig. 3.— **Left panel:** The spectra of accelerated electrons and protons corresponding to the timescales shown in Figure 2 (right). The dotted curves give the spectra at the acceleration site (LT) and the dashed curves give the thick target equivalent spectra of escaping particles. The solid (black) line gives the shape of the background (injected) particle distribution. The hatched areas show the energy ranges for production of frequently observed ranges of HXRs (for electrons) and gamma-ray lines (for protons). Spectral features occur at the intersections and divergences of these timescales (circle and square signs shown here and in Fig. 2; right). **Right panel:** The dependence of electron spectrum on the $\mathcal{W} \propto \tau_p^{-1}$. Higher $\mathcal{W}$'s produce harder spectra and more acceleration vs heating (see PL04).

The spectral characteristics of the particles arise from the interplay among the timescales shown above. Figure 3 (left) shows the corresponding spectra of electrons and protons at the LT ($N_{\rm LT}$, dotted) and the equivalent FP thick target spectra (dashed lines; see *e.g.* Petrosian 1973, Park, Petrosian & Schwartz 1997)

$$N_{\rm FP}(E) = \dot{E}_L^{-1} \int_0^E N_{\rm LT}(E') T_{\rm esc}^{-1}(E') dE'. \tag{12}$$

Spectral breaks occur at energies (circles and squares) when different terms become important. As evident, in general, SA by PWT produces a "quasi-thermal" and a harder non-thermal component; *i.e.* it both "heats" the plasma and accelerates particles. As also seen in the right panel of Figure 3, the relative strength of the two components depends sensitively on the intensity $\mathcal{W} \propto \tau_p^{-1}$ of the PWT. For higher densities of turbulence the spectra are harder. In addition, the LT spectra are dominated by the thermal component with a steep non-thermal component, while the FP spectra are harder with little or non-thermal part. These agree with the observed features discussed below. For low $\mathcal{W}$, *e.g.* during the build-up and decay phases of a flare, one expects only plasma heating with essentially no non-thermal component (see below and PL04).

3.3. Application to Solar Flares

Ultimately observations must determine the validity of the models. As described below there have been extensive comparisons of the SA model with observations. To our knowledge, there have not been similarly detailed comparisons for electric field or shock acceleration.

3.3.1. Radiative Signatures of Electrons

Spatial Structure and Evolution: The most direct evidence for the presence of PWT is observations by *Yohkoh* of distinct LT impulsive HXR emission (Masuda et al. 1994, Masuda 1994), which have been shown to be common to almost all *Yohkoh* (Petrosian, et al. 2002) and *RHESSI* (Liu et al. 2004) flares. Petrosian & Donaghy (1999) have also shown that these observations require an enhanced pitch angle scattering to confine the particles near the LT. Coulomb collisions cannot be this agent because of high losses they entail. The most likely scattering agent is PWT, which can also accelerate particles. Figure 4 (left) shows a cartoon of the reconnection and acceleration site for a flaring loop with the red foam representing the PWT produced during reconnection. As reconnection proceeds larger closed loops are formed below this site. This simple picture then predicts a gradual rise of the LT source accompanied with a continuous increase in separation of the FPs. Most strong flares are complex and involve multiple (or arcade) of loops (*e.g.* July 23,

time for particles to cross the turbulent region of size L (see PL04).

2002 flare; Krucker et al. 2003), which obscures the simple single loop behavior. In weaker flares, on the other hand, this behavior is lost in the noise. *RHESSI* has detected a strong X-class flare (Nov. 3, 2003) consisting of a single loop which shows exactly this behavior (Liu et al. 2004, see Fig. 4, middle). Similar motion but only for the LT source has been seen in several other *RHESSI* flares (see *e.g.* Sui & Holman 2003). In rare cases, specially when the FP sources are weak or occulted by the sun, one can see a double LT source (Fig. 4 right, from Liu 2007, see also Sui et al. 2005) as envisioned by the cartoon on the left.

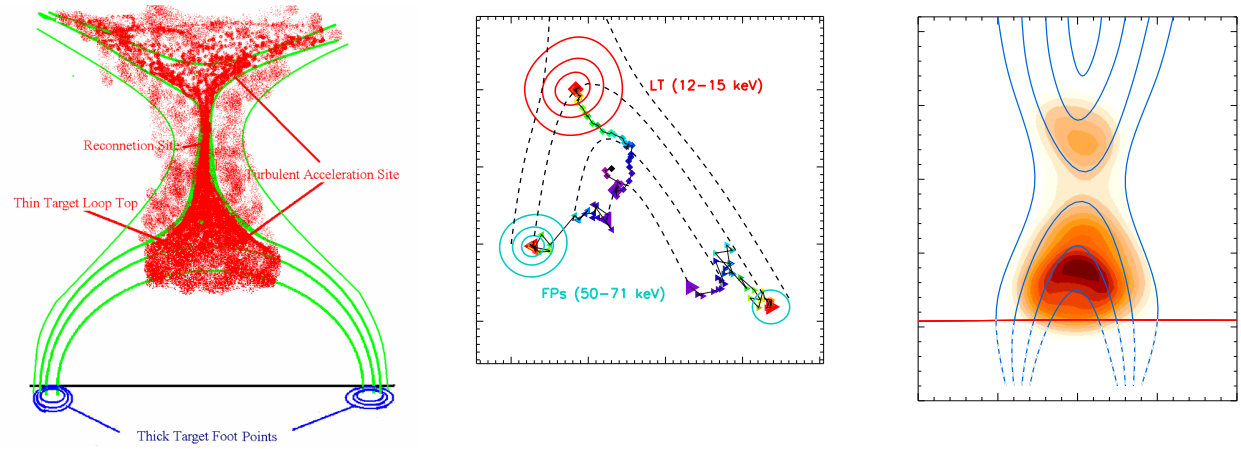

Fig. 4.— **Left panel:** A schematic representation of the reconnecting field forming closed loops and open coronal field lines. The red foam represents PWT. **Middle panel:** Temporal evolution of LT and FP HXR sources of Nov. 3, 2003 flare. The symbols indicate the source centroids and the colors show the time with a 20 sec interval, starting from black (09:46:20 UT) and ending at red (10:01:00 UT) with contours for the last time. The curves connect schematically the FPs and the LT sources for three different times showing the expected evolution for the model at the left; from Liu et al. (2004). **Right panel:** Image of flare of April 30, 2002, with occulted FPs showing an elongated LT source with two distinct peaks as expected from the model in the left (see Liu et al. 2008). The curves representing the magnetic lines (added by hand) show the presumed occulted FPs below the limb (red line); from Liu (2007).

Spectral Characteristics: Observations over a broad energy range (*e.g.* Marschhäuser et al. 1994, Dingus et al. 1994, and Park, Petrosian, & Schwartz 1997) show several spectral breaks. Petrosian et al. (1994) have shown that these features present in the so-called electron-dominated flares cannot be due to transport or optical depth effects and are natural consequences of the SA by PWT (Park et al. 1997). Early high resolution observations (Lin et al. 1981) showed spectral steepening below a few tens of keV, which is also consistent with the SA model (Hamilton & Petrosian 1992). *RHESSI*'s imaging spectroscopy has clarified this situation considerably. In general, during the impulsive phase the spectra are dominated by a non-thermal component, with the LT always softer than the FPs, and there is a quasi-thermal component (mostly from the LT) occurring sometimes before the impulsive phase and always during the decay phase, which is in concordance with the features of the accelerated electrons described above. Figure 5 shows these observed characteristics of the LT and FP sources for two typical *RHESSI* x-ray flares fitted with theoretical spectra from the SA model.

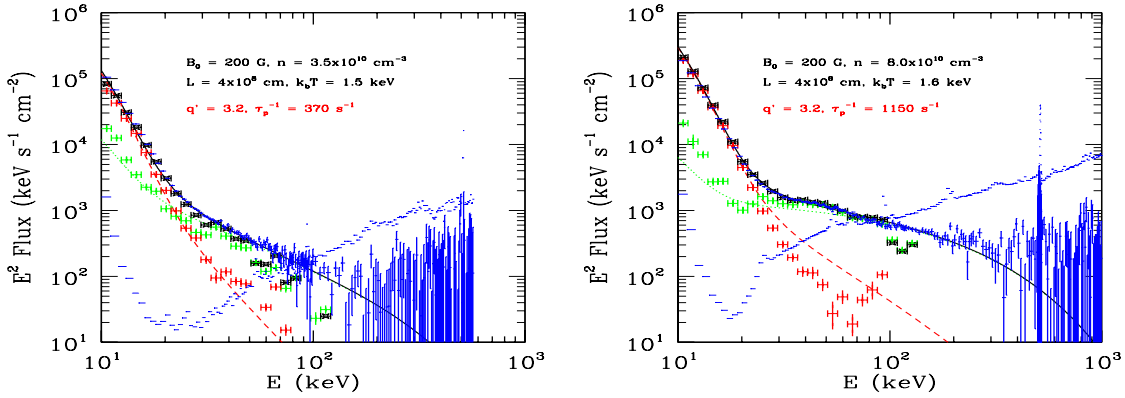

Fig. 5.— **Left panel:** A fit to the total (black), FP (green) and LT (red) spectra of the first HXR pulse of the Sep. 20th 2002 flare observed by *RHESSI*. Model parameters are indicated in the figure. The dashed and dotted lines are model spectra from equations (3) and (12) showing the presence of a quasi-thermal (LT) and a non-thermal (mostly FPs) component. The solid line gives the sum of the two. The blue dashes indicate the level of the background radiation. **Right panel:** Same as the left panel but for the second HXR peak. Note that compared with the model parameters for the first HXR pulse, both the gas density and the turbulence energy density increase during the second pulse, resulting more thermal emission and harder photon spectra.

Spectral Evolution: It has also been known for sometime that some observations disagree with the model where all the released energy goes directly to non-thermal electrons during *the impulsive phase*. Among these are precursor soft X-ray emission referred to as *preheating* and a slower than expected temperature decline in the decay phase (see, *e.g.* McTiernan et al. 1993)[6]. In several *RHESSI* limb flares Jiang et al. (2006) find that during the decay phase the (resolved) LT source continues to be confined; it does not extend to the FPs as one would expect if the evaporation fills the whole loop with hot plasmas. Moreover, the observed energy decay rate is calculated to be higher than the radiative cooling rate but much lower than the (Spitzer 1961) conduction rate. The latter and the confinement of the LT source require suppression of the conduction and a continuous energy input. PWT can be the agent for both. It can reduce the scattering mean free path and energize the plasma continuously during the decay phase (albeit at a diminishing rate).

The observed spectral breaks and the temporal evolution also agree with the model results discussed above. During the build-up and decay (*i.e.* pre- and post-impulsive) phases when the level of PWT is low it only manages to "heat" the plasma with little acceleration into a non-thermal tail. Particle acceleration begins in earnest during the impulsive phase when the rate of reconnection and production of PWT rises and then falls after reaching high levels. During this rise and fall the spectra undergo soft-hard-soft evolution as observed in most flares.

[6]The expected Neupert (1968) relation also does not seem to hold (see Dennis & Zaro 1993; Veronig et al. 2005).

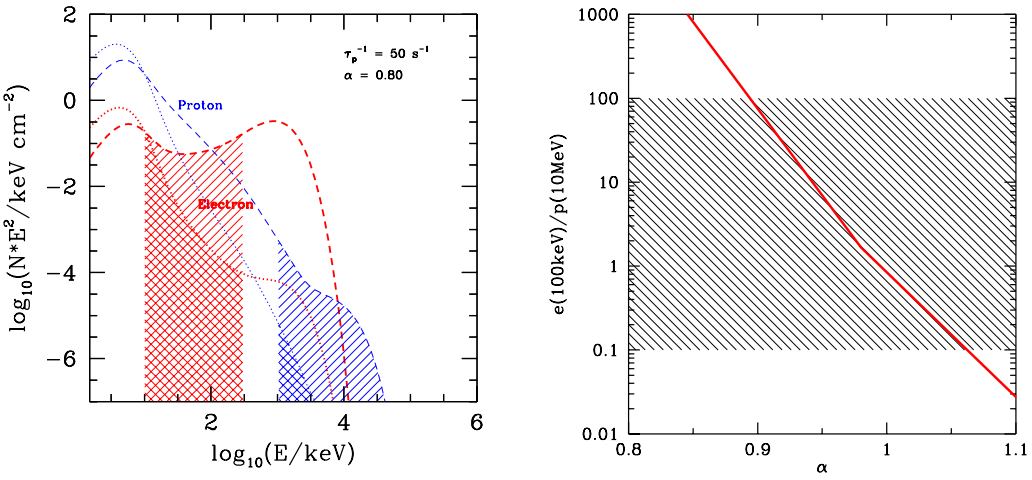

Fig. 6.— **Left panel:** Same as left panel of Figure 3 but for a different α showing the dependence of relative electro and proton spectra on α. **Right panel:** Variation with α of the ratio of the energies of the accelerated electrons and protons in the spectral energy range shown by the shade region in the left panel.

3.3.2. Radiative Signatures of Protons and Ions

Observations of gamma-ray lines in larger solar flares provide evidence for acceleration of protons and ions. The SA model has been the working hypothesis here as well (see works by Ramaty and collaborators earlier, and Murphy and Share recently). For these flares the ratio of energy content of accelerated electrons to protons (in the hatched range of Fig. 3, left) ranges from 100 to 0.03 (Mandzhavidze & Ramaty 1996); this ratio is larger in electron dominated flares. On the other hand, simple theoretical models, for example acceleration by Alfvén waves commonly used, favor a much smaller ratio. PL04 show that with a more complete treatment of the wave-particle interaction a barrier appears for proton acceleration, which reduces the number of accelerated protons dramatically, in a way that the above ratio is very sensitive to the plasma parameter α in equation (11). Figure 6 shows this dependence. The left panel is same as the left panel in Figure 3 but for a smaller α. The right panel shows the variation with α of the ratio of the energy of electron to protons (in the respective shade region). One consequence of this is that the proton acceleration will be more efficient in larger loops, where the B field is weaker, and at late phases, when due to evaporation n is higher. This can explain the offset of the centroid of the gamma-ray line emissions from that of HXRs seen by *RHESSI* (Hurford et al. 2003). It can also account for the observed delay of nuclear line emissions relative to HXR emissions seen in some flares (Chupp et al. 1990). This trend is also true for other ions because the acceleration barrier moves to lower energies with decreasing α. or In general, higher densities, lower magnetic fields favor acceleration of ions versus the electrons and can explain the diversity in their relative observed values both at the flare site and in the interplanetary space.

3.3.3. SEP Spectra and Abundances

It is commonly believed that the observed relative abundances of ions in SEPs favor a SA model (*e.g.* Mason et al. 1986 and Mazur et al. 1992). More recent observations have confirmed this picture (see Mason et al. 2000, 2002, Reames et al. 1994 and 1997, and Miller 2003). There are similarities and differences among the spectra and abundances of different ions from event to event. One of the most vexing problem of SEPs has been the enhancement of ^{3}He in the so-called *impulsive events*, which sometimes can be $3-4$ orders of magnitude above the photospheric value. As stated at the outset these events, which we prefer to call ^{3}He-rich rather than impulsive, is the focus of thees proceedings. There has been many attempts to explain this and the related enhancements of heavy ions observations. This will be the subject of the next sections.

4. Enhancement of ^{3}He and Heavy Ions

As stressed in the previous chapters one of the most puzzling aspects of observations of SEPs is the enhancement of ^{3}He and heavy ions relative to their photospheric values in many of the so-called impulsive events. Over the years there has been many attempts to account for these observations. In this section we first present a brief review of past attempts at tackling this problem and then describe how well the SA model described above can account for these aspects of solar flares.

4.1. Past Works

Most of the proposed models, except the Ramaty and Kozlovsky (1974) model based on spalation (which has many problems), rely on resonant wave-particle interactions to produce the observed enhancement. The earliest theoretical models addressing this issue are those of Ibragimov and Kocharov (1977) and Fisk (1978).

- Ibragimov and Kocharov claim that under the influence of Langmuir turbulence the plasma ion temperature will increase linearly in time with a rate proportional to the momentum diffusion coefficient. Citing another paper they also claim that the diffusion rate will be proportional to the Coulomb charge times the gyrofrequency which favors heating of ^{3}He relative to protons and ^{4}He. A second stage of acceleration with a velocity or energy threshold for all particles will then accelerate a larger fraction of ^{3}He ions than ^{4}He and proton. The parameters of the model can be adjusted to obtain the observed enhancements.

- Fisk's model relies on the fact that ^{3}He can interact more efficiently than ^{4}He with (electrostatic hydrogen-cyclotron) waves having frequency between proton and ^{4}He gyrofrequencies. Damping of these waves preferentially heats ^{3}He ions. There are two major shortcomings in

this model. The main difficulty here is that to have sufficient overheating one requires excitation of waves close to ^{3}He gyrofrequency (=4/3 of ^{4}He) which can be produced if electron to proton temperature ratio and/or the ^{4}He to hydrogen ratio are large. Again, this model does not answer the full question of production of enhanced population of non-thermal ^{3}He ions. It leaves this to a secondary process which also must satisfy the requirement of having a threshold velocity for acceleration near the thermal velocity of the heated ^{3}He ions. Fisk also tries to explain the enhancement of the heavy elements the same way but relying on the resonant interactions with the second gyro-harmonics. This aspect also may not be correct.

- Temerin and Roth (1992) use essentially same idea but with electromagnetic hydrogen-cyclotron waves. They carry out numerical simulation based on somewhat artificial model (waves moving down the variable field lines and ^{3}He ions moving up that interact when the resonant condition is satisfied). They also produce some heating of ^{3}He ions but do not discuss the spectrum nor the expected ratio of ^{3}He /^{4}He . Again, like in the Fisk model first and second harmonics ($n = 1$ and 2) are invoked for ^{3}He and heavy ion heating, respectively. However, there is no estimate of heavy ion fluxes. Curiously, Fisk is not acknowledged except in passing mentioning only the shortcoming mentioned above.

- Miller and Viñas (1993) expand on Temerin and Roth work by inclusion of more waves and more-realistic plasma conditions. Most of this paper is devoted to calculating the growth rate and dispersion relation of waves excited by a thermal, isotropic "beam" of electrons superimposed as a bump in a somewhat cooler thermal plasma consisting of electrons, protons and alpha particles. The acceleration of particles is carried out using orbit calculations for test particles. As in the above works it merely leads to some heating of iron and ^{3}He ions. It is then stated that this heating is more than what they expect to occur for other ions (*e.g.* CNO) and ^{4}He , respectively. The required "beam" densities are much higher than those required for describing the Type III radio emission. (These authors provide a good summary and analysis of earlier works).

- Zhang (1995) uses a more refined version of the Fisk model and evaluates the degree of overheating of ^{3}He ions relative to ^{4}He . In addition he includes a simple calculation of subsequent acceleration by a "Fermi" process and derives a general spectrum. However, these spectra are not compared with the observed ones; they are essentially exponential in form and will not fit well to the observations. Instead he evaluates the abundance ratios and plots these versus some important parameters which can be compared with the gross features of the observations.

- Paesold, Kallenbach and Benz (2003) rely on a somewhat different aspect of the acceleration process. In their model waves are excited by anisotropic distribution of electrons (so-called Fire Hose Instability) with a growth rate that is slightly higher at the ^{3}He gyrofrequency than that of ^{4}He . It is then claimed that this can lead to a much larger (exponential) difference in the wave energy density at the corresponding frequencies. With a larger wave density

at its disposal ^{3}He acceleration proceed more rapidly. The acceleration method is used is the same as in Miller and Viñas discussed above. However, unlike the above works this paper addresses the spectral differences between ^{3}He and ^{4}He, but there is no comparison with actual observed spectra. This model also predicts that there should be i) many more accelerated protons (which is swept under the rug invoking some energy limitation) and ii) a suppressions of iron and other heavier ions (whose Q/A is less than that of ^{4}He or CNO) instead of the observed enhancements.

In summary the common theme among all these models is that they use the difference between the Q/A of ^{3}He and ^{4}He and require some non-Maxwellian electron distribution to excite the waves that then preferentially heat ^{3}He ions. Some also require very special conditions. The outcomes of all these works are in general some differential heating with the actual acceleration often relegated to a subsequent process. There is little or no comparison with observed spectra and every model requires some additional factor to explain the enhancements observed for iron and heavier ions.

In contrast to this the model proposed by Liu, Petrosian and Mason (2004, 2006) based on the SA by PWT (PL04) treats heating and acceleration as a single process, can reproduce some of the observed spectral features, and can account for the range of the observed enhancement. On the other hand, at this stage of its development this model does not address the details of the production of the waves or turbulence and relies on injection, presumably during the reconnection process, and the subsequent cascade and damping of the waves. Some of the salient results of this model are described next.

4.2. Enhancements and Stochastic Acceleration

In this section we describe the role the SA model described in the previous sections can play in the enrichment of ^{3}He and other elements. The formalism described above can be applied to the acceleration of all ions in the same way used to fit the radiative signatures of the accelerated electrons and protons to observations. All the results presented below are based on acceleration by PPWs and most of the results are from Liu et al. (2004, 2006).

Figure 7 (left) shows the dispersion relation near the proton and ^{4}He gyrofrequencies and the resonant conditions for two different energies of ^{3}He and ^{4}He ions. The presence of fully ionized ^{4}He (about 8% of protons) in the background plasma divides the Alfvén wave-proton cyclotron branch into two distinct modes which we have labeled proton cyclotron (PC) and He cyclotron (HeC) branches. Because of the gap between these two modes at low values of the wavevector k, low energy ^{4}He ions resonate only with the HeC branch while ^{3}He ions can resonate with both branches and are accelerated more efficiently. The right panel of this figure depicts the relevant time scales showing the much shorter acceleration time for ^{3}He than ^{4}He at low energies. This is the primary cause of the ^{3}He enrichment.

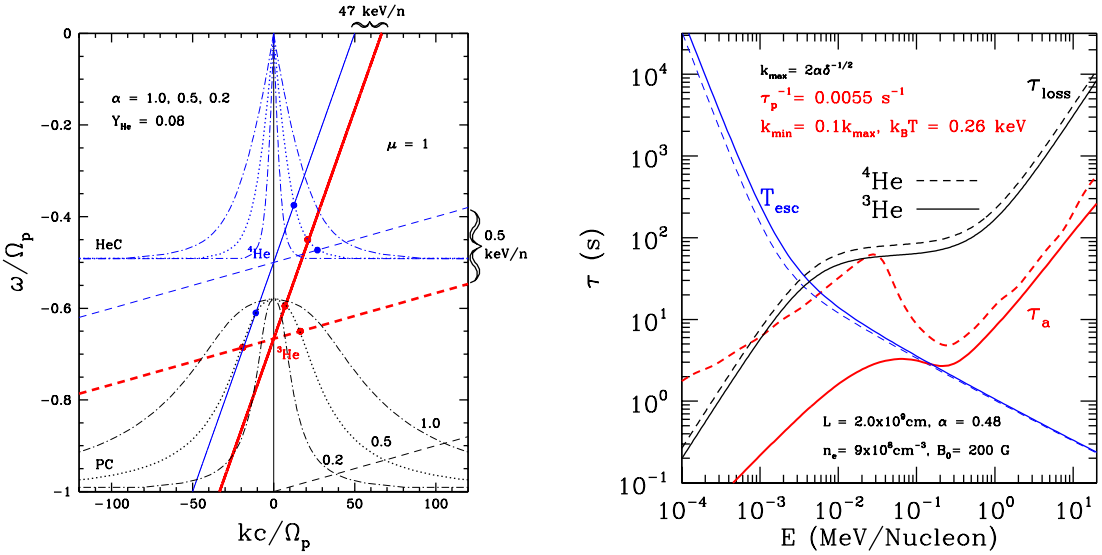

Fig. 7.— **Left panel:** Dispersion relations for parallel propagating waves and resonance conditions for ^{3}He and ^{4}He for the specified energies and three different values of α. Note that the resonance lines for ^{3}He start (at k=0) at its gyrofrequency (divided by $\gamma \sim 1$), which is larger (in absolute value) than that of ^{4}He. As a result at low energies ^{3}He has more resonant intersections (filled circles) than ^{4}He. Right panel: Acceleration, escape and energy time scales for ^{3}He an ^{4}He. The main difference here is the shorter acceleration time for ^{3}He at lower energies because of its stronger interactions with waves.

As a result of this more efficient acceleration most ^{3}He ions are accelerated to form a non-thermal distribution. While ^{4}He ions are heated up forming a low energy quasi-thermal bump with only a small fraction reaching to high energies. Figure 8 shows model spectra fitted to two ^{3}He rich SEP events displaying the above features. Another result of the efficient acceleration is that one expects a high degree of acceleration of ^{3}He even in smaller events such that the ^{3}He/^{4}He abundance ratio is expected to decrease with increasing fluence of the event. This is what is seen (see Fig. XXX in Chapter 2) and is demonstrated in the right panel of Figure 8 where we show spectra for three different values of the acceleration rate τ_p^{-1}. For higher rates more of the ^{4}He ions in the quasi-thermal tail reach into the non-thermal tail decreasing the ^{3}He enrichment and the ^{3}He/^{4}He ratio.

The dependence of ^{3}He enrichment on model parameters is further demonstrated in Figure 9. The most influential parameter is the acceleration rate $\tau_p^{-1} \propto \mathcal{W}$ and there is some variation with α at low acceleration rates. There is little dependence on the (unknown) spectral parameters of the turbulence. The trend and the range of the variations presented here are in agreement with the observations described in chapter 2. It remains to be seen whether or not the spectral trend presented in Figure 8 (middle and right) also agrees with observations. It should also be possible to use the observed distributions of ^{4}He and ^{3}He fluences or peak fluxes to further test this promising model and constrain its parameters. This will require a sample of events with known selection

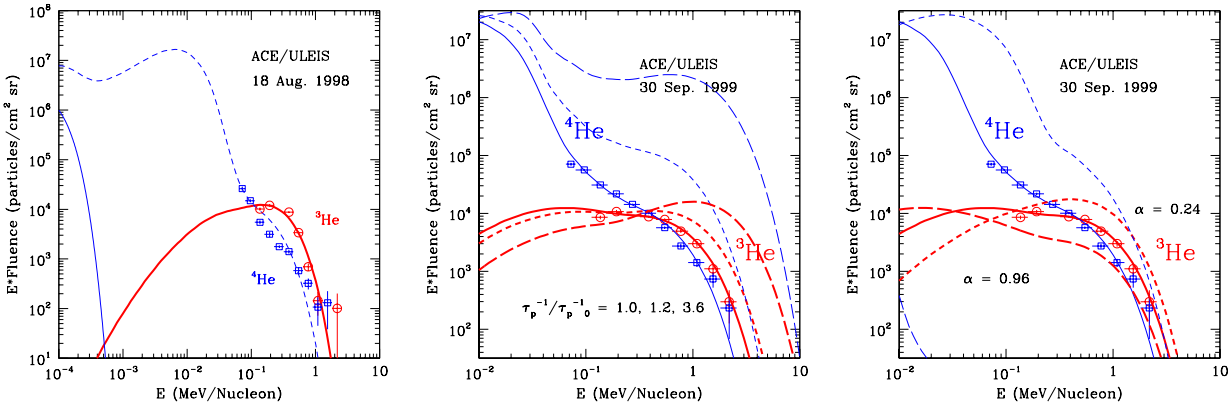

Fig. 8.— Fits to ^{3}He and ^{4}He spectra of two ^{3}He rich SEP events. Note that because of the shorter acceleration time of ^{3}He at low energies most of the ^{3}He is accelerated into super thermal tail while most of ^{4}He ions are heated up to a high 'temperature' quasi-thermal distribution with only a smaller fraction forming a non-thermal tail. The middle and right panels also show two additional sets of model spectra with somewhat higher and lower values of τ_p^{-1}, which is proportional to the turbulence energy density or the rate of acceleration, and α, respectively.

criteria and observational biases.

5. Summary and Discussion

We have discussed possible mechanism of accelerations in solar flares and SEPs, and pointed out that in all mechanisms plasma waves and turbulence play a major role. We have then argued that in solar flares the most likely mechanism is stochastic acceleration by plasma waves and turbulence and have demonstrated that the predictions of this model are consistent with most of the observed flare radiative signatures. We have also shown that the observed ^{3}He enrichment and the spectra of ^{3}He and ^{4}He can be described by such a model without requiring any special conditions. The same model that successfully describes the observed radiation can also account for this long standing puzzle. Unlike previous models, which addressed only the enhancement (without detailed comparison with observed spectra) and required special conditions and/or two stage acceleration, the model presented here neither requires special conditions nor another acceleration mechanism.

Another important problem of SEP observations is enhancement of abundances of heavier ions with the enhancement increasing with ionic mass or mass-to-charge ratio described in Chapter 2. Here the situation is more complicated because of the uncertainty about the charge state of these ions and the observations of dependence of the charge state on the ion energy discussed in previous chapters. These observations also favor acceleration in relatively high densities of the lower corona, where the stochastic acceleration invoked here occurs. Figure 10 (left) shows abundances of a large number of ion species obtained from a composite of many SEP events (red points, Mason, private

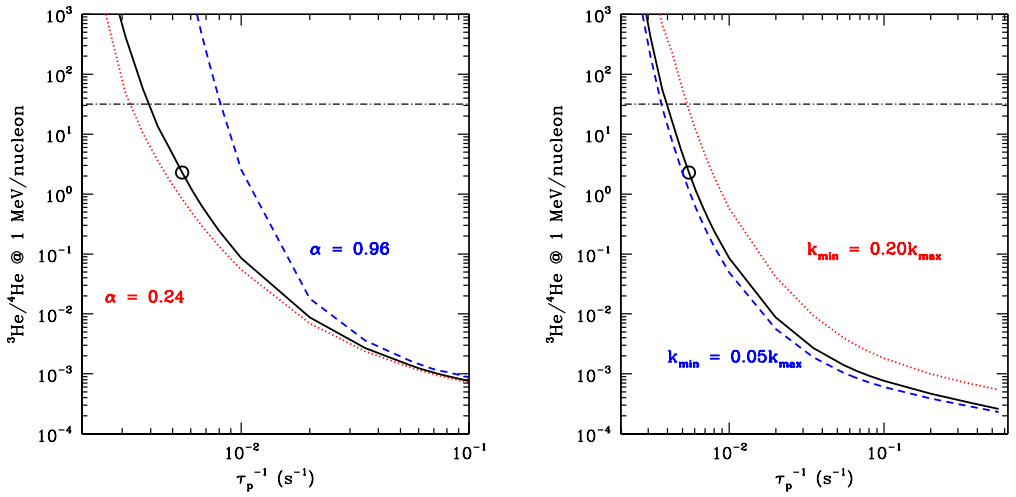

Fig. 9.— Variation with acceleration rate (or level of turbulence) of the ^{3}He/^{4}He fluence ratio at 2 MeV per nucleon for different values of α (left) and the spectral break wave vector $k_{\max}$ (right). The black lines are for best fit values of $\alpha = 0.46$ and $k_{\min} = 0.1k_{\max}$ for the 30 Sep. 1999 event shown in Figure 8 (middle and left). These curves show the possibility of obtaining a large range of the ratio of ^{3}He/^{4}He and that the main characteristics of turbulence affecting this ratio is the energy density $\mathcal{W} \propto \tau_p^{-1}$ with smaller effect due to α and a relatively insignificant effect due to unknown details of the turbulence spectrum (see Liu et al. 2006).

communication). The black points and the line show our preliminary attempt (Liu & Petrosian in preparation) to fit these observations. Fits to protons ^{3}He and ^{4}He are as above and in plotting the line we have assumed a charge of 16 for all the elements above iron.

This scenario in the form presented here will encounter difficulty with the observations of the intermediate ions (*e.g.* CNO). We note that most of the observed spectra refer to the event fluence. The models described above are based on the time-independent (or the steady state) equations. This is valid when the acceleration time is shorter than the dynamic time scale of the event (*e.g.* event duration), in which case the steady state results are good approximation. A more accurate analysis requires a time-dependent analysis. Figure 10 (right) shows a preliminary result from such a model (East, Petrosian & Liu, in preparation) from such a model. The dashed lines show the time evolution of the spectrum of ^{16}O and the solid green line the time integrated spectrum appropriate for the fluence spectrum shown by the green squares. This model seems to provide a reasonable fit (except at low energies where the uncertainties are large) for both ^{16}O and ^{4}He . Clearly more data and more detailed model are required to put this comparison on the same footing as those described above for electrons, protons and He ions.

6. REFERENCES

Amato, E., & Blasi, P. 2005, MNRAS, 364, 76

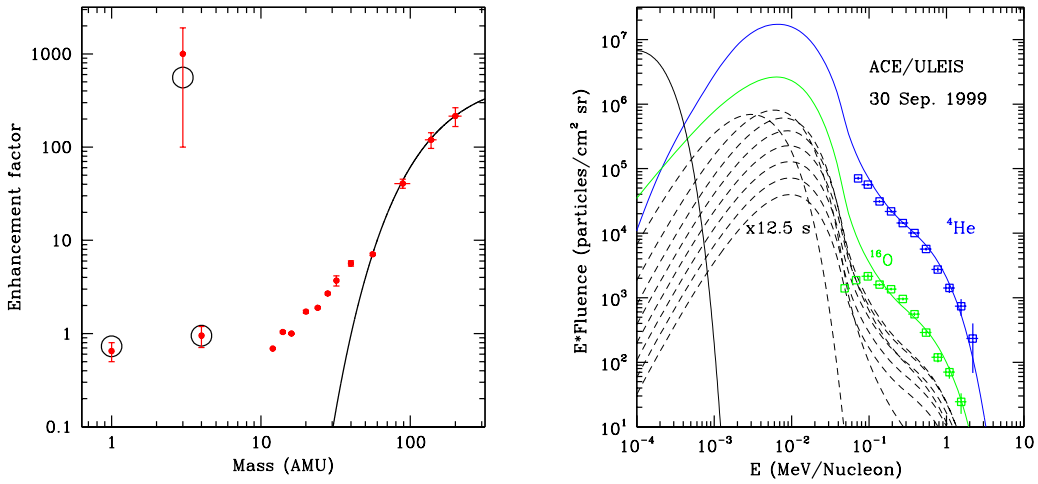

Fig. 10.— **Left panel:** A preliminary fit by the SA model to different ion enhancements obtained from a composite of many events (red points from Mason, private communication). The open circles and the black curve are the model results assuming a charge of 16 for all elements heavier than iron (Liu & Petrosian, in preparation). This, of course, is inappropriate for intermediate ions where the time-independent model described here cannot describe the observations. **Right panel:** A preliminary result from a time-dependent treatment showing the evolution of ^{16}O (dashed lines) spectrum and the time integrated spectrum (solid green) fitted to observed spectrum of fluences of ^{16}O and ^{4}He for a typical event.

André, Mats 1985, *J. Plasma Phys.*, 33, 1

Boris, J. P., Dawson, J. M., Orens, J. H., & Roberts, K. V. 1970, *Phys. Rev. Lett.*, 25, 706

Cassak, P. A., Drake, J. F. & Shay, M. A. 2006, *Ap. J.*, 644, L145

Chandran, B. 2005, *Phys. Rev. Lett.*, 95, 265004

Cho, J., & Lazarian, A. 2002, *Phys. Rev. Lett.*, 88, 245001

Cho, J., & Lazarian, A. 2006, *Particle Acceleration by MHD Turbulence*, *Ap. J.*, 638, 811

Chupp, E. L. 1990, *Science*, 250, 229

Cranmer, S. R., & van Ballegooijen, A. A. 2003, *Ap. J.*, 594, 573

Dennis, B. R., & Zarro, D. M. 1993, *Solar Phys.*, 146, 177

Dingus, B. L. et al. 1994, *AIP Conf. Proc.* eds. J. M. Ryan & W. T. Vestrand, 294, 177

Drake, J. F., Paper presented at *Krakow Conference on Relativistic Jets*, June 2006

Ellison, D. C., Decourchelle, A, & Ballet, J. 2005, *Astr. & Astrophys.*, 429, 569

Farmer, A., Goldreich, P. 2004, *Ap. J.*, 604, 671

Fisk, L. A. 1978, *Ap. J.*, 224, 1048

Giacalone, J. 2005, *Ap. J. (Letters),* 628, L37

Goldreich, P., & Sridhar, S. 1995, *Ap. J.*, 438, 763

Goldreich, P., & Sridhar, S. 1997, *Ap. J.*, 485, 680

Hamilton, R. J. & Petrosian, V. 1992, *Ap. J.*, 398, 350

Holman, G. D. 1985, *Ap. J.*, **293**, 584

Holman, G. D. 1996a, *BAAS*, 28, 939

Holman, G. D. 1996b, *AIP Conf. Proc.* eds. R. Ramaty et al., 374, 479

Hoshino, M., Paper presented at *COSPAR Scientific Assembly* Beijing, July 2006

Hurford, G. J. et al. 2003, *Ap. J.*, 595, 77L

Ibragimov, I. A. & Kocharov, G. E. 1977, Proc. 15th Int, Cosmic Ray Conf. (Plovdiv), 11, 340

Iroshnikov, P., 1963, *Astron. Zh.*, 40, 742 (English version: 1964, Sov. Astron., 7, 566)

Jiang, Y. W. et al. 2006, *Ap. J.*, 638, 1140

Jones, F. C. 1994, *Ap. J. Suppl.*, 90, 561

Jokipii, R. J. 1987, *Ap. J.*, 313, 842

Kraichnan, R., 1965, Phys. Fluids, 8, 1385

Lin, R. P. et al. 1981, *Ap. J. (Letters),* 251, L109

Lithwick, Y., & Goldreich, P. 2001, *Ap. J.*, 562, 279

Litvinenko, Y. E. 2003, *Solar Phys.*, 212, 379

Liu, S., Petrosian, V., & Mason, G. 2004, *Ap. J. (Letters),* 613, L81

Liu, S., Petrosian, V., & Mason, G. 2006, *Ap. J.*, 634, 462

Liu, W. et al. 2004, *Ap. J.*, 611, 53L

Liu, W. 2007, from PhD thesis, Stanford University

Luo, Q. & Melrose, D. 2006; astro-ph/0602295

Kulsrud, R.M. 2005, *Plasma Physics for Astrophysics*, Princeton Univ. Press

Mandzhavidze, N., & Ramaty, R. 1996, *BAAS*, 28, 858

Marschhäuser, H. et al. 1994, *AIP Conf. Proc.* eds. J. M. Ryan & W. T. Vestrand 294, 171

Mason, G. M. et al. 1986, *Ap. J.*, 303, 849

Mason, G. M., Dwyer, J. R., & Mazur, J. E. 2000, *Ap. J.*, 545, 157L

Mason, G. M. et al. 2002, *Ap. J.*, 574, 1039

Masuda, S. et al. 1994, *Nature*, 371, 495

Masuda, S. 1994, University of Tokyo, Ph.D. Thesis

Mazur, J. E. et al. 1992, *Ap. J.*, 401, 398

McTiernan, J. M. et al. 1993, *Ap. J. (Letters),* 416, L91

Miller, J. A. 2003, *COSPAR Colloquia Series* Vol. 13, 387

Miller, J. A.,LaRosa, T.N., & Moore, R.L. 1996, *Ap. J.*, 445, 464

Miller, J. M. & Reames, D. V. 1996, *AIP Conf. Proc.* eds. R. Ramaty et al., 374, 450

Miller, J.A.& Viῖvas, A. F. 1993, ApJ, 412, 386

Neupert, W.M. 1968, *Ap. J.*, 153, L59

Park, B. T., Petrosian, V., & Schwartz, R. A. 1997, *Ap. J.*, 489, 358

Paesold, G., Kallenbach, R. & Benz, A. O. 2003, ApJ 582, 495

Petrosian, V. 1973, *Ap. J.*, 186, 291

Petrosian, V., & Donaghy, T. Q. 1999, *Ap. J.*, 527, 945

Petrosian, V., Donaghy, T. Q., & McTiernan, J. M. 2002, *Ap. J.*, 569, 459

Petrosian, V., & Liu, S. 2004, *Ap. J.*, 610, 550 **PL04**

Petrosian, V., McTiernan, J.M., & Marschhäuser, H. 1994, *Ap. J.*, 434, 744

Petrosian, V,, Yan, H. & Lazarian, A. 2006, *Ap. J.*, 644, 603

Pryadko, J., & Petrosian, V. 1997, *Ap. J.*, 482, 774

Pryadko, J., & Petrosian, V. 1998, *Ap. J.*, 495, 377

Pryadko, J., & Petrosian, V. 1999, *Ap. J.*, 515, 873

Ramaty, R. & Kozlovsky, B. 1974, ApJ 193, 729

Reames, D. V., Meyer, J. P., & von Rosenvinge, T. T. 1994, ApJS, 90, 649

Reames, D. V. et al. 1997, *Ap. J.*, 483, 515

Sui, L., & Holman, G. D. 2003, *Ap. J. (Letters),* 596, L251

Sui, L., Holman, G. D., & Dennis, B. R. 2005, *Ap. J.*, 626, 1102

Swanson, D. G. 1989, *Plasma Waves* (New York: Academic Press)

Temerin, M. & Roth, I. 1992, ApJ 391, L105

Tsuneta, S. 1985, *Ap. J.*, 290, 353

Veronig, A. M. et al. 2005, *Ap. J.*, 621, 482

Yan, H., & Lazarian, A. 2002, *Phys. Rev. Lett.*, 89, 2881102

Zenitani, S. & Hoshino, M. 2005, *Ap. J.*, 618, L111

Zhang, T. X. 1995, ApJ, 449, 916

Zhou, Y., & Matthaeus, W.H. 1990, *J. Geophys. Res.* 95, 14881